

# On the influence of downwelling winds on the Chesapeake Bay outflow

Arnoldo Valle-Levinson

*Center for Coastal Physical Oceanography, Old Dominion University, Norfolk, Virginia, USA*

Kamazima M.M. Lwiza

*Marine Sciences Research Center, The University at Stony Brook, NY, USA*

## ABSTRACT

With the purpose of studying the hydrography and flow structure off the mouth of the Chesapeake Bay, a series of transects were sampled continuously with a 600 kHz acoustic Doppler current profiler (ADCP) and a thermosalinograph during late September 1995. Hydrographic (CTD) stations were combined with underway measurements and occupied every 4 km along the transects to look at the vertical structure of the density field. This is the first time an ADCP has been towed in the waters off the Chesapeake Bay mouth. The study was carried out at the end of a two-day period of northeasterly winds. The surface salinity distribution showed that winds kept a well-defined Chesapeake Bay plume within a few kilometers from the coast. Near-bottom salinity fields displayed weaker horizontal gradients than the near-surface field. The ADCP observations yielded excellent resolution of the flow field from which a subtidal distribution was inferred. The subtidal near-surface flow showed a spatially coherent southward component in the area of observation in response to the downwelling winds. The southward coastal ambient flow advected the turning region of the plume to the south of the mouth of the estuary, which was consistent with numerical model results. The region of influence by the plume could be defined from the subtidal flows by an area where the difference between the near-surface and near-bottom flows was large. This area, off the Chesapeake Bay mouth, overlapped with that of subtidal flow divergence as calculated with the near-surface subtidal flow. Within the region of plume influence, the balance was probably semigeostrophic with modifications by friction in the along-flow direction. Outside that region, the momentum balance was apparently dominated by friction.

## 1 INTRODUCTION

The study of estuarine discharges onto the continental shelf has received widespread attention as these discharges transport land-derived and estuarine-derived materials to the coastal oceans. The Chesapeake Bay outflow is a typical example of a buoyant discharge from a wide estuary. This discharge is derived from an annual mean river input of 2400 m<sup>3</sup>/s (Hargis, 1981). The hydrography of the Chesapeake Bay plume has been described in several studies by Boicourt (1973; 1981), and Boicourt *et al.* (1987). These studies have shown that under the influence of downwelling winds, or northeasterly winds blowing onshore, the buoyant discharge from the estuary is restricted to a narrow band to the south of the estuary's mouth. With upwelling winds, or southwesterly winds blowing offshore, the buoyant water extends off the mouth of the Chesapeake Bay, forming a wide turning region.

Despite of having a relatively good idea of the modifications to the plume's density field by wind forcing, knowledge on the response of the flow field is restricted to records of scattered moored instruments. Comprehensive descriptions of the flow field have only been described with numerical models (e.g. Chao and Boicourt, 1986; Chao, 1988; Zhang *et al.*, 1987; Weaver and Hsieh, 1987; Oey and Mellor, 1993). Prior to the present study, no measurements had been made of the spatial structure of the flow field in the Chesapeake Bay outflow region. The main objective of this study is to describe the flow structure associated with a weak plume under the influence of downwelling winds. This constitutes the first effort that studies the Chesapeake Bay plume using underway current measurements obtained with an acoustic Doppler current profiler (ADCP). These observations help validate models of plume dynamics under downwelling winds.

## 2 DATA COLLECTION

A series of transects (Fig. 1) was sampled with a 600 kHz broadband acoustic Doppler current profiler (ADCP) during 26 hours from September 25 to 26, 1995. Table 1 summarizes the details of the ADCP data collection. The ADCP was mounted on a catamaran and towed from the National Oceanic Atmospheric Administration (United States) ship R/V Ferrel. This was the first time an ADCP was towed in the waters off the Chesapeake Bay mouth. Simultaneously to the current velocity measurements, near-surface temperature and salinity were recorded every 10 seconds with a Sea Bird thermosalinograph (SBE-1621). Underway measurements were combined with Conductivity-Temperature-Depth (CTD - Sea Bird SBE-25) stations, occupied every 4 km along the transects, to elucidate the vertical structure of the density field. The sampling grid extended for approximately 60 km in the alongshelf direction from Cape Charles, Virginia, to False Cape, at the border between Virginia and North Carolina, and 20 km in the cross-shelf direction.

Acoustic Frequency	600 kHz
Beam Angle	30°
Ping Rate	0.95 Hz-PBT, 2 Hz-PDT & PET
Sampling Interval	30 s
Blanking Interval	1 m
Center of First Bin	2 m
Beam Length	0.5 m
Bottom Track	Yes, during the entire study
Data Acquisition	RDI Transect
Navigation	GPS

Table 1. ADCP Specifications

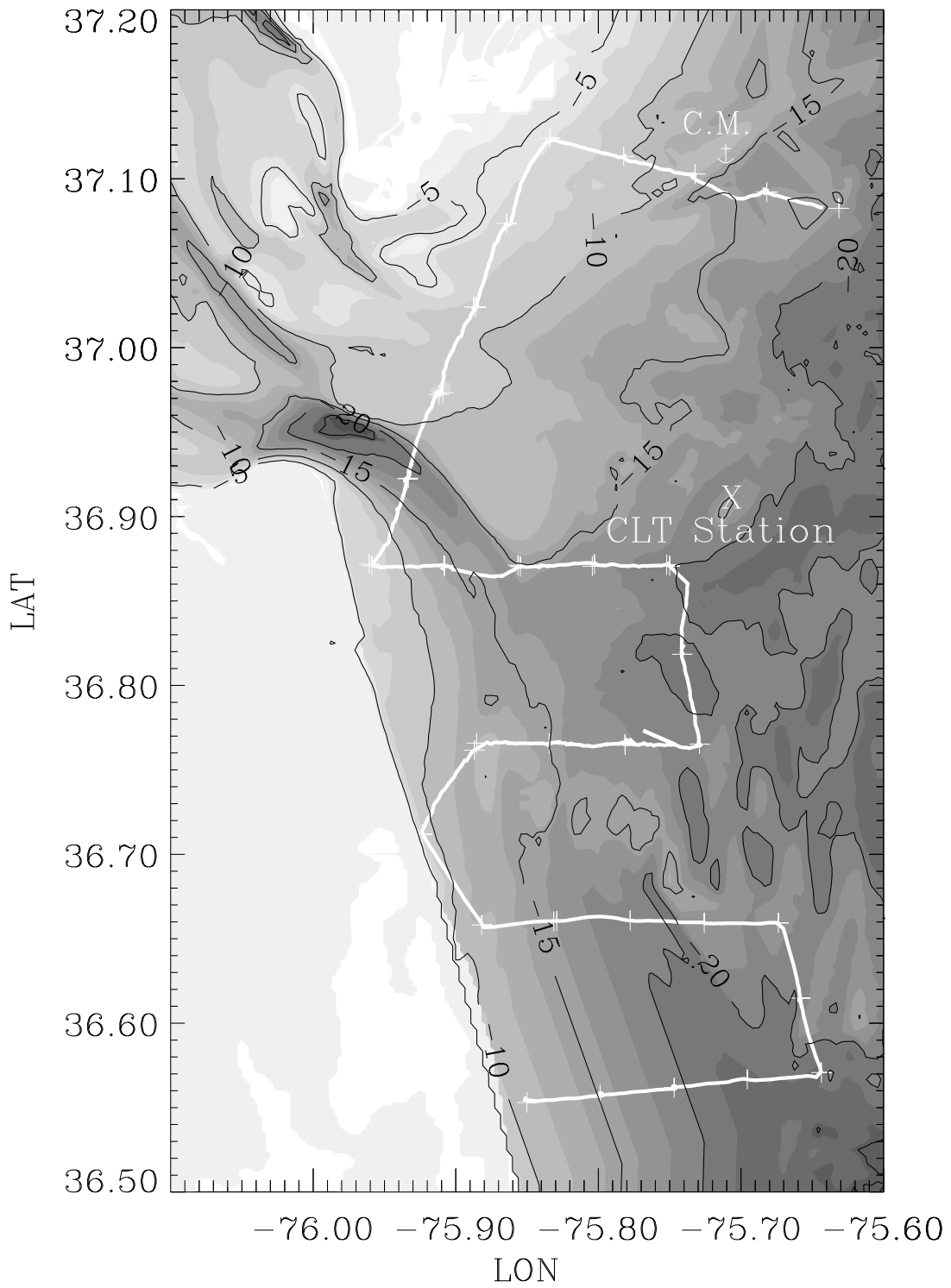


Figure 1. Study area with location of transects (thick white line), of current meter (C.M.) mooring, of wind data (station CLT), and of CTD stations ('+'). Bathymetry is contoured at 2 m intervals.

Prior to the beginning of the underway measurements, a mooring with near-surface and near-bottom current meters was also deployed. The instruments used were SensorData 6000 (see Valle-Levinson, 1995 for an explanation of the instruments). The records from these instruments were used to look at the tidal variations of the flow at one location, which provided a guide in the process of separating the tidal and non-tidal signals from the ADCP data. Wind data from the Chesapeake Light Tower (Fig. 1) were used to relate the observed velocity and density fields to wind forcing conditions.

### **3 DESCRIPTION OF OBSERVATIONS**

The measurements of flow and density fields were carried out in early autumn, when river discharge to the Chesapeake Bay is at its minimum (Valle-Levinson and Lwiza, 1997a). It also coincided that the observations were obtained at the end of a two-day period of northeasterly, or downwelling, winds (Fig. 2a). These winds caused a predominant southward current during our survey (Figs. 2b and 2c). The tidal current barely reversed the wind-induced current during the first tidal cycle of ADCP observations. The current meter records were obtained under vertically homogeneous conditions and were used to validate the procedure of separating tidal and non-tidal contributions to the ADCP data in the vicinity of the mooring.

The low freshwater discharge and the wind forcing previous to and during the study reflected the low buoyancy-high mixing hydrographic regime in the lower Chesapeake Bay as proposed by Valle-Levinson and Lwiza (1997a). The surface salinity showed relatively high values (greater than 28) and a Chesapeake Bay plume confined to within a few kilometers (approximately 5-10 km) from the coast (Fig. 3a). Near-bottom salinity fields displayed weaker horizontal gradients than the near-surface field (Fig. 3b) and the difference between surface and bottom salinities was typically 2 in the region closest to the coast. This salinity field suggested the decoupling of near-surface fluid from near-bottom dynamics, at least near the mouth of the bay. The near-surface and near-bottom subtidal flows derived from the ADCP measurements provided further evidence of this decoupling as discussed later.

The current velocity profiles obtained with the ADCP yielded excellent resolution of the flow field along the sampling track. The raw near-surface flow (Fig. 3a) exhibited the characteristic pattern of the mean flow of a wide estuary plume: turning region of the outflow due to Coriolis acceleration, transition to a coastal current with noticeable flow convergence, and formation of a coastal current downstream of the region of convergence. The unprocessed measurements displayed large differences between the near-surface and near-bottom tidal flows at the southernmost transects. These current velocity profiles are, however, tidally aliased. Therefore, the signal related to the tidal currents had to be isolated from the observations in order to examine the ambient field. The technique of detiding is described next.

#### ***3.1 Detiding of ADCP and Surface Salinity Data***

The ADCP data bins closest to the surface (at approximately 2 m depth) and bottom (at 85% of the total depth), along with the near-surface continuous salinity data from the thermosalinograph, were subjected to a least squares fit of a semidiurnal tidal wave with the help of predefined base functions. Near-bottom salinity was not detided because the CTD casts did

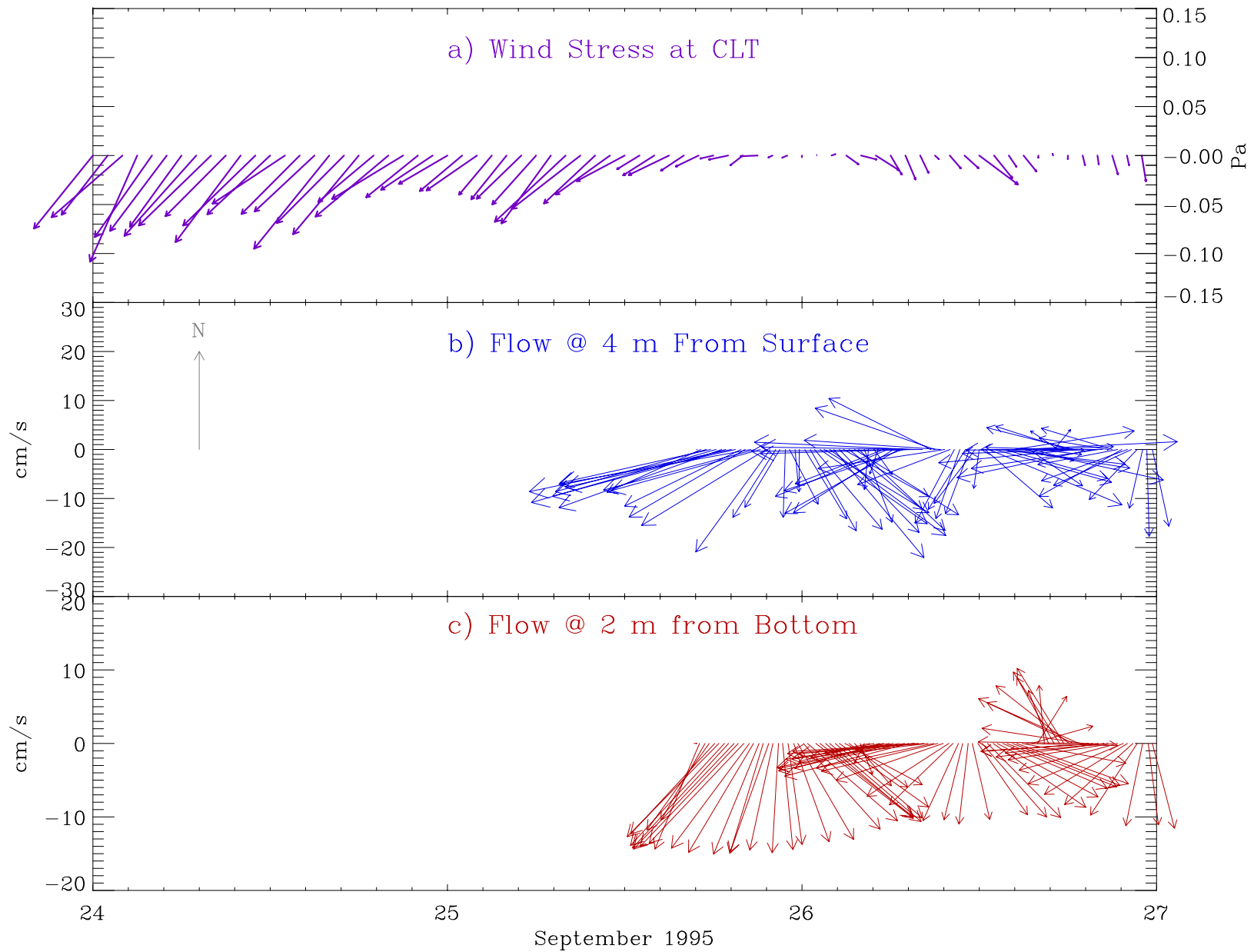


Figure 2. (a) Wind stresses (Pa) at CLT using the oceanographic convention (vectors point in the direction toward which the wind blows). (b) and (c) Current velocities during the period of ADCP measurements.

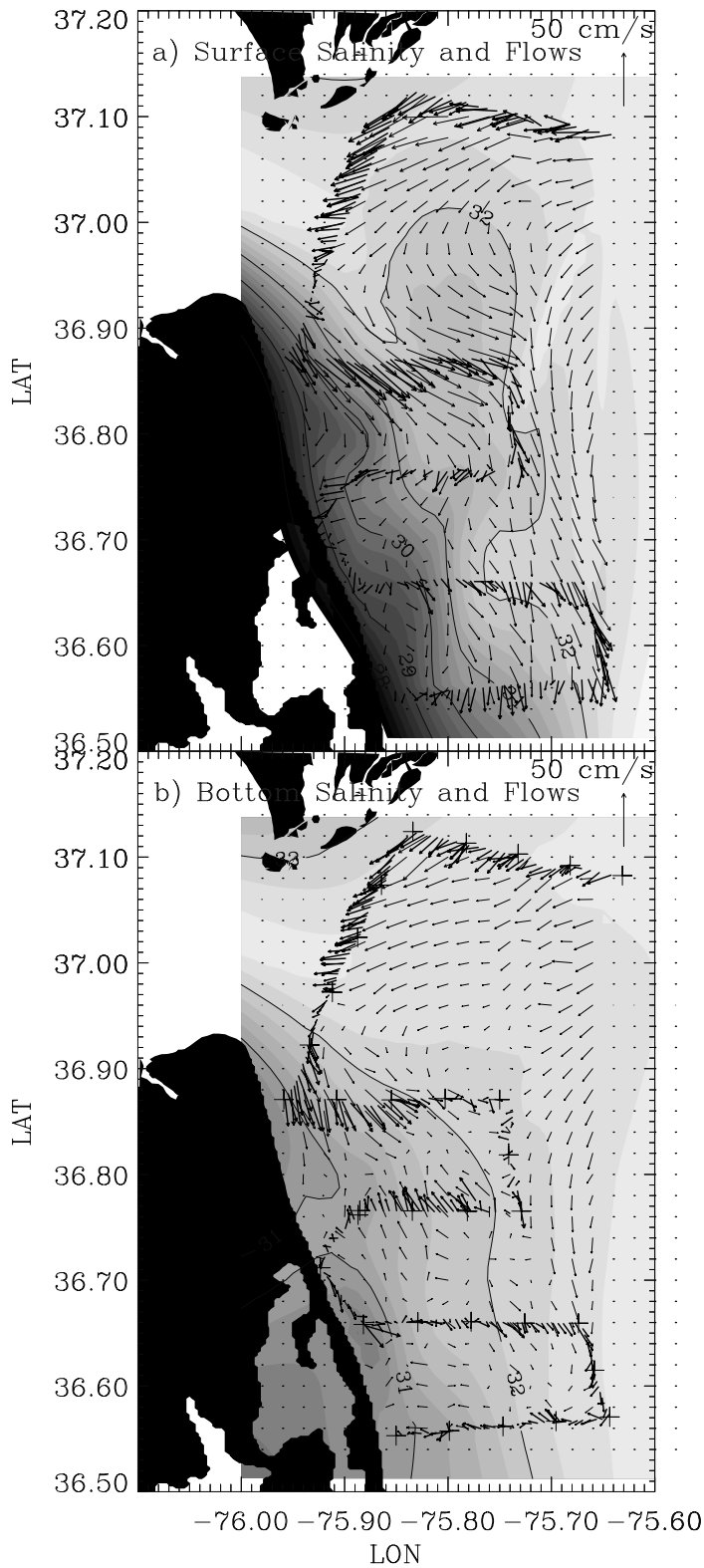


Figure 3. Instantaneous salinity (shaded contours) and flow (vectors) fields as measured with CTD and ADCP. The flow fields are plotted along the ship track and at regular grid points, where they were interpolated from the observations along the track. Salinity values are contoured at increments of 1. (a) Near-surface, and (b) near-bottom fields.

not yield enough spatial resolution to produce reliable results as the number of degrees of freedom is small. The detiding method and the errors associated with it have been outlined by Candela *et al.* (1992), and Wong and Münchow (1995). The method is presented more explicitly here. To obtain the fit, it was assumed that each observed velocity component,  $u_{io}(x,y,t)$ , and the near surface salinity signals varied in horizontal space  $(x,y)$  and were formed of a subtidal component  $u_{im}$  plus a semidiurnal (period = 12.42 hrs) tidal component plus noise, *i.e.*,

$$u_{io}(x,y,t) = u_{im}(x,y) + a_i(x,y) \cos(\omega_{M2} t) + b_i(x,y) \sin(\omega_{M2} t) + \text{noise}(x,y,t), \quad (1)$$

where  $\omega_{M2}$  is the frequency of the lunar semidiurnal tidal component ( $2\pi/12.42$  h). The subtidal flow component (or salinity), and the functions  $a_i(x,y)$  and  $b_i(x,y)$ , are given by:

$$\begin{aligned} u_{im}(x,y) &= \sum_1 \alpha_1(x,y) \phi_1(x,y), \\ a_i(x,y) &= \sum_1 \beta_1(x,y) \phi_1(x,y), \\ b_i(x,y) &= \sum_1 \gamma_1(x,y) \phi_1(x,y). \end{aligned}$$

The parameters  $\alpha_1, \beta_1, \gamma_1$ , are to be found by minimizing the least square error between observations and fit at each of the "I" nodes located at  $(x_1, y_1)$ .  $\phi_1(x,y)$  are base functions that, for this application, have been chosen as biharmonic splines (Wong and Münchow, 1995), *i.e.*,

$$\phi_1(x,y) = \{(x - x_1)^2 + (y - y_1)^2\} \{\ln[(x - x_1)^2 + (y - y_1)^2]^{1/2} - 1\}.$$

Differentiating the squared error  $(u_{io} - u_{i\text{fit}})^2$  with respect to each unknown parameter  $\alpha_1, \beta_1, \gamma_1$ , and equating to zero, yields a set of 3L equations, where L is the total number of nodes. The set of 3L equations can be arranged in the following matrix form to solve for  $\alpha_1, \beta_1, \gamma_1$  (contained in X):

$$F X = O \quad (2).$$

Matrix  $F$  is symmetric and has the following general form:

$$\begin{bmatrix} \sum_N \phi_1 \phi_1 & \dots & \sum_N \phi_L \phi_1 & \sum_N \phi_1 \phi_1 \sin \omega t & \dots & \sum_N \phi_L \phi_1 \sin \omega t & \sum_N \phi_1 \phi_1 \cos \omega t & \dots & \sum_N \phi_L \phi_1 \cos \omega t \\ \vdots & & \vdots & & & \vdots & & & \vdots \\ & \sum_N \phi_L \phi_L & & & & & & & \\ & & \sum_N \phi_1 \phi_1 \sin^2 \omega t & & & \sum_N \phi_1 \phi_1 \cos \omega t \sin \omega t & & & \dots \\ & & & \ddots & & & & & \vdots \\ & & & & \sum_N \phi_L \phi_L \sin^2 \omega t & & & & \\ & & \sum_N \phi_1 \phi_1 \sin \omega t \cos \omega t & \dots & & \sum_N \phi_1 \phi_1 \cos^2 \omega t & & & \\ & & & \vdots & & & & & \vdots \\ & & & & & & & & \sum_N \phi_L \phi_L \cos^2 \omega t \end{bmatrix}$$

The vector  $X$  is  $[\alpha_1, \dots, \alpha_L, \beta_1, \dots, \beta_L, \gamma_1, \dots, \gamma_L]$ ; and the vector  $O$  has the elements  $[\sum_N u_{io} \phi_1, \dots, \sum_N u_{io} \phi_L, \sum_N u_{io} \phi_1 \sin \omega t, \dots, \sum_N u_{io} \phi_L \sin \omega t, \sum_N u_{io} \phi_1 \cos \omega t, \dots, \sum_N u_{io} \phi_L \cos \omega t]$ . The solution  $X$  is obtained by inverting the matrix  $F$ .

### 3.2 Fitted Data

The least squares fit obtained with equations 1-2 and 5 nodes, reproduced the most prominent variations of both components of the observed flow (Fig. 4a, b) and of the surface salinity. The fit depends on the position of the nodes, *i.e.*, variations to the node location yield different subtidal and tidal flow fields. The node locations chosen here were optimized in such a way that the noise had zero mean and variance that was a small fraction (less than 10%) of the variance of the observations (Wong and Münchow, 1995). In addition, the optimal node locations were chosen for those that reproduced the tidal currents from moored instruments.

The subtidal component  $u_m$  of the fit contains the currents produced by winds, density gradients, and oscillations longer than 12.42 hrs. Therefore, the subtidal flow field thus obtained, reflected the wind and buoyancy forcing during the period of study. The subtidal near-surface flow and salinity calculated along the ship track (Fig. 1), were interpolated to a grid with 1.77 km spacing in the east-west direction ( $0.02^\circ$  lon), and 2.22 km in the north-south direction ( $0.02^\circ$  lat). This grid spacing was chosen arbitrarily. The interpolation was carried out through the construction of a Delaunay triangulation that produces interpolated values computed from nearby points only. This is an intrinsic function in the data processing package Interactive Data Language (IDL).

The gridded subtidal salinity field at the surface (Fig. 5) showed a relatively thin ( $< 10$  km from the coast) band of buoyant water along the coast to the south of the Chesapeake Bay mouth. This band is constrained by the internal radius of deformation ( $\sim 6$  km) and by the downwelling winds. Comparing the mouth of the bay (width of outflow) to the radius of deformation yields a Kelvin number greater than 1, which indicates that rotation effects play a major role in the dynamics of the plume (Wiseman and Garvine, 1995; Garvine, 1995). On the same figure 5, the smooth character of the subtidal flow is due to the biharmonic splines and does not necessarily reflect actual conditions. This near-surface subtidal flow showed a southward component ( $V$ ) that was coherent throughout the region of study. This was consistent with the moored velocity observations and was most probably related to the downwelling wind forcing. In fact, a complex regression between the wind velocity ( $W_x, W_y$  in m/s) and the near-surface subtidal flow ( $U, V$  in m/s) during the study period yielded the following fit

$$\begin{aligned}U &= 0.04 W_x \\V &= -0.04 + 0.04W_y\end{aligned}$$

where the  $x$  and  $y$  subscripts denote east-west and north-south components, respectively. The flow pattern produced by this fit was very similar to that shown in Figure 5 and explained 90% of the spatial variability of the subtidal flow (Valle-Levinson and Lwiza, 1997b). The large

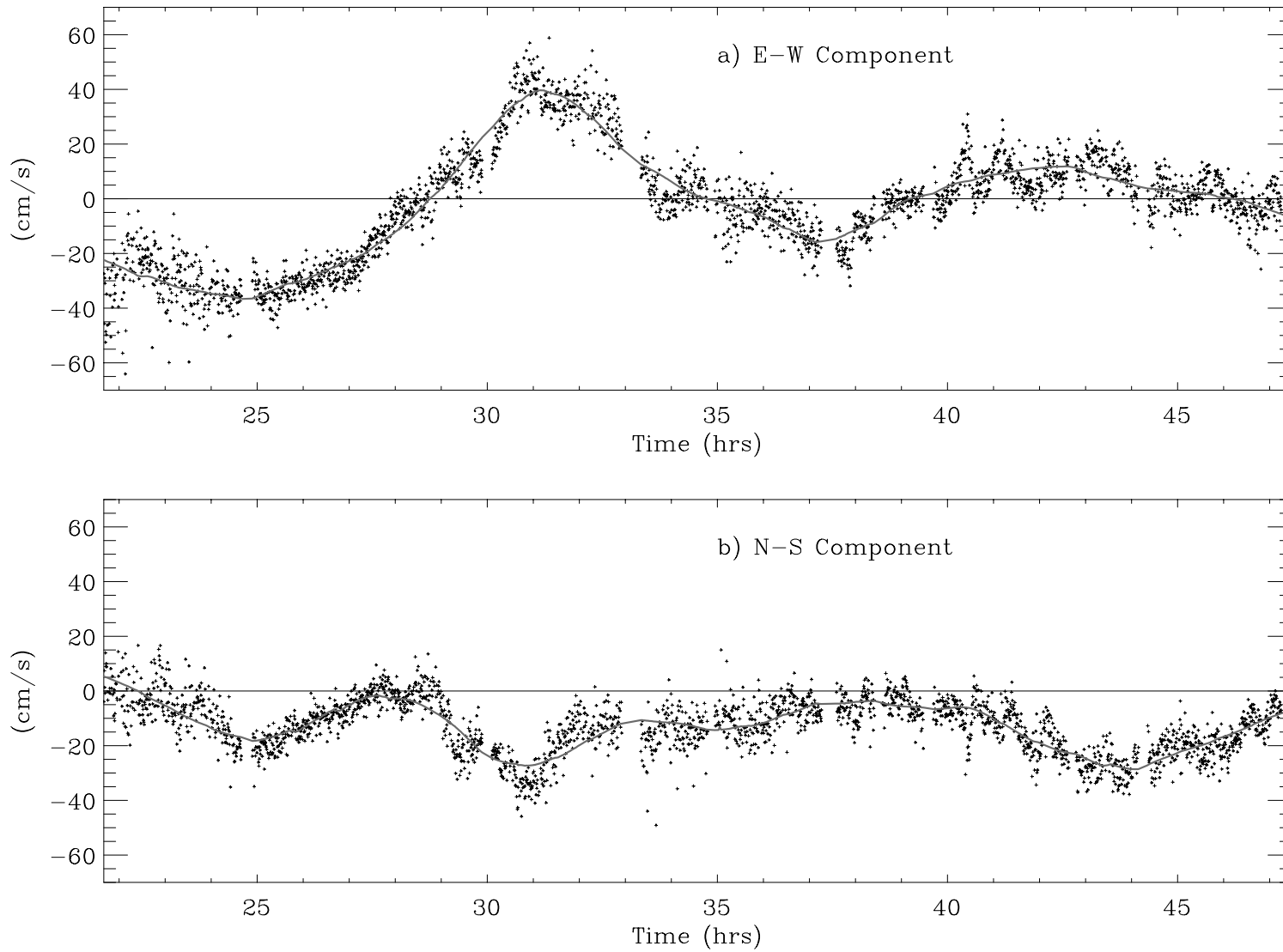


Figure 4. Comparison between observed components of the flow (dots) and fitted values (smooth, continuous line). (a) East-west component, and (b) north-south component.

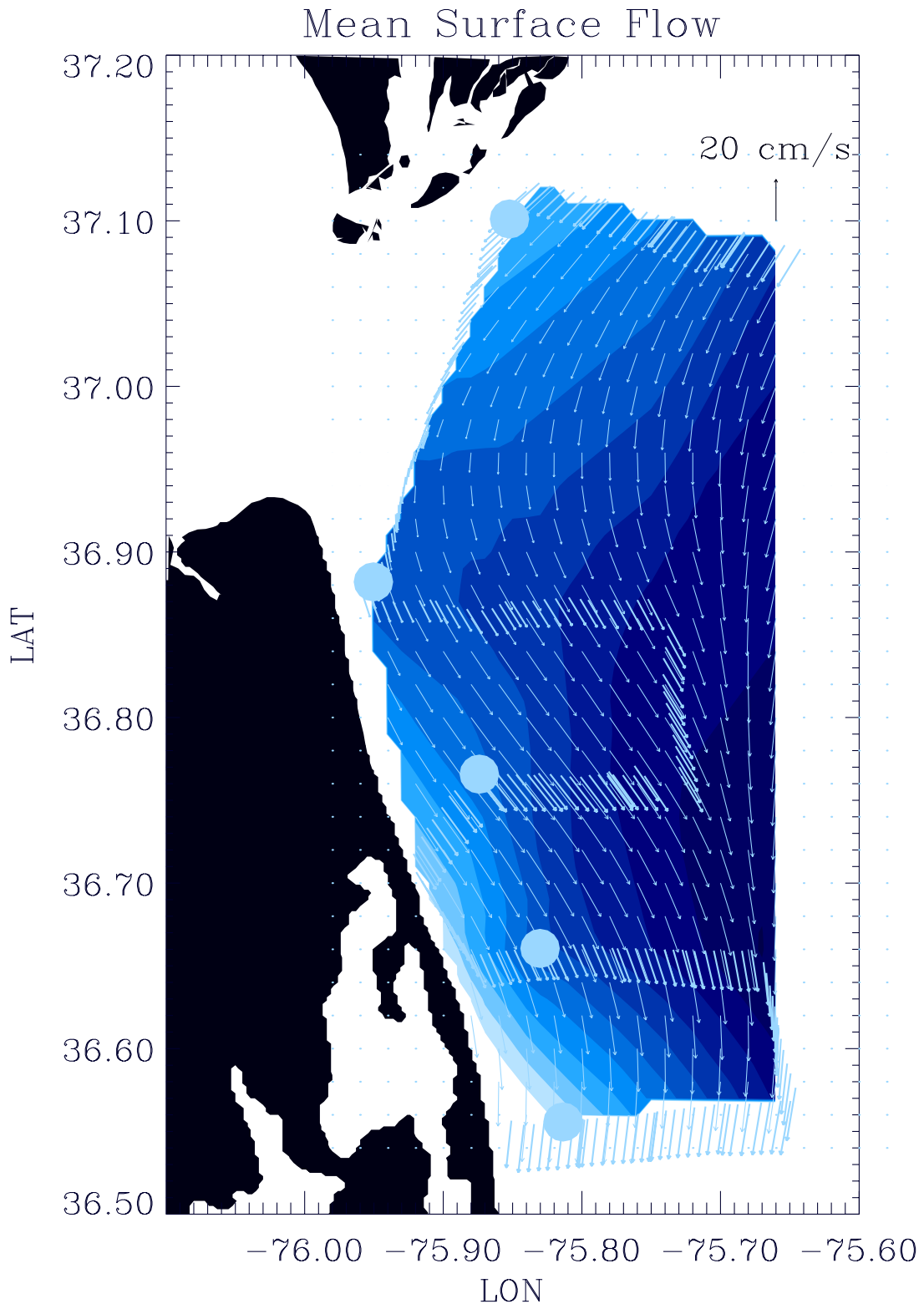


Figure 5. Subtidal near-surface (2 m deep) salinity (shaded contours) and flow (vectors). The nodes that anchored the fit are shown as filled circles.

variability explained by the fit indicates that wind forcing was mostly responsible for the subtidal flow observed under these weak plume conditions. The  $-0.04$  offset of the fit to the  $V$  component is related to the southward ambient flow.

Another important and innovative result of this study is that the turning region of the outflow plume is advected southward of the mouth by the along-shelf southward flow. This behavior is consistent with numerical results (Valle-Levinson *et al.*, 1996) of a plume discharging to a shelf where a coastal flow is active (Fig. 6a). The ambient flow plunges underneath the plume at the zone where they encounter and the plume thickness increases as a consequence of mixing (O'Donnell, 1990). The ambient flow is quite influential to the dynamics of the plume because the suppression of the coastal flow allows the offshore spreading of the plume (Fig. 6b).

The subtidal near-bottom flow showed regions where it opposed the near-surface flow and regions where it flowed in approximately the same direction (Fig. 7a). Near the mouth of the Chesapeake Bay the subtidal near-bottom flow was directed into the estuary suggesting decoupled dynamics from the near-surface fields. This is the area of possible influence of the density pressure gradients on the subtidal flow thus generating estuarine-like circulation. Southward of this zone apparently dominated by baroclinic forcing, the near bottom flow diverged and became aligned to the direction of the wind forcing, which suggested barotropic flow. The subtidal near-bottom flow also showed the formation of anticyclonic circulation associated with a bathymetric shoaling of 2 m with respect to the surrounding depth. The region of inflow near the mouth, the divergence south of this region, and the anticyclonic circulation are features that are consistent with the results obtained by Norcross and Stanley (1967) with bottom drifters (Fig. 7b). This adds validity to the detided results, in addition to the fact that the noise had an average of almost zero and a small variance relative to the variance of the observed near-bottom flow.

The baroclinic character of the subtidal flows was determined by subtracting the near-bottom from the near-surface N-S component of the subtidal flows. This estimate gave an idea of the possible regions of decoupled dynamics from surface to bottom. The areas of greatest vertical difference in the subtidal flows (Fig. 8a) appeared right off the mouth of the Chesapeake Bay, within what should be the plume region, *i.e.*, the zone of strongest baroclinicity. This region was probably where the plume was detached from the bottom. The detachment was confirmed by the salinity measurements obtained off the mouth of the bay (not shown). Another region with large vertical differences in subtidal flow developed above the shoaling that generated the near-bottom anticyclonic circulation. The former zone must have been a result of the density field, and the latter reflected bathymetric effects. These zones of greatest shear coincided with the regions where the N-S subtidal component pointed in opposite directions, as shown on Figure 8a. The regions of large vertical differences in subtidal flow could have produced instabilities in the density field (Wiseman and Garvine, 1995). The hydrographic observations did not have the sufficient spatial resolution to verify this.

The separation in distinct regions by the subtidal shears suggests different dynamical implications for each. Within the plume region, near the mouth of the estuary, the circulation must be estuarine-like, *i.e.*, the momentum balance must be semigeostrophic with modifications

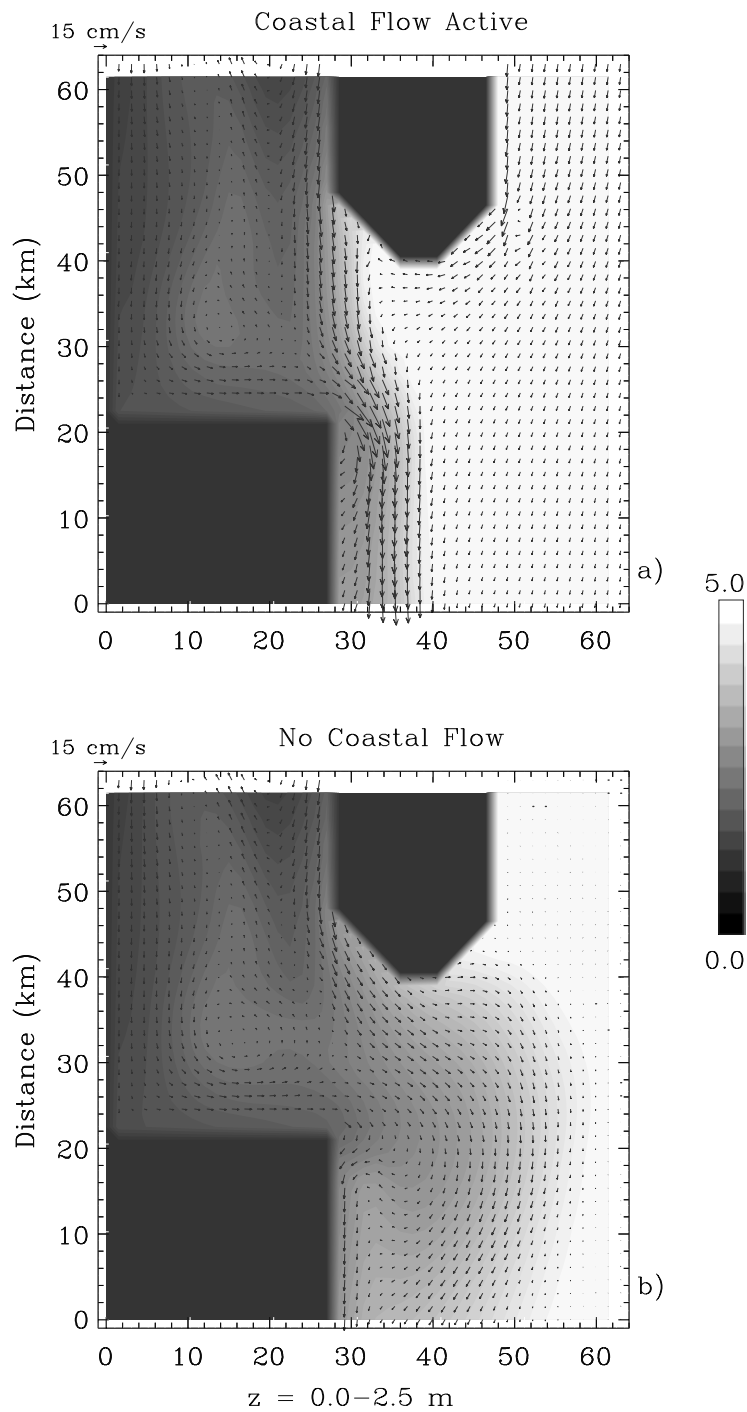


Figure 6. Surface fields of salinity (shaded) and flows (vectors) obtained numerically by Valle-Levinson *et al.* (1996) for (a) southward coastal flow active, and (b) no coastal flow. The color bar indicates the salinity contrast.

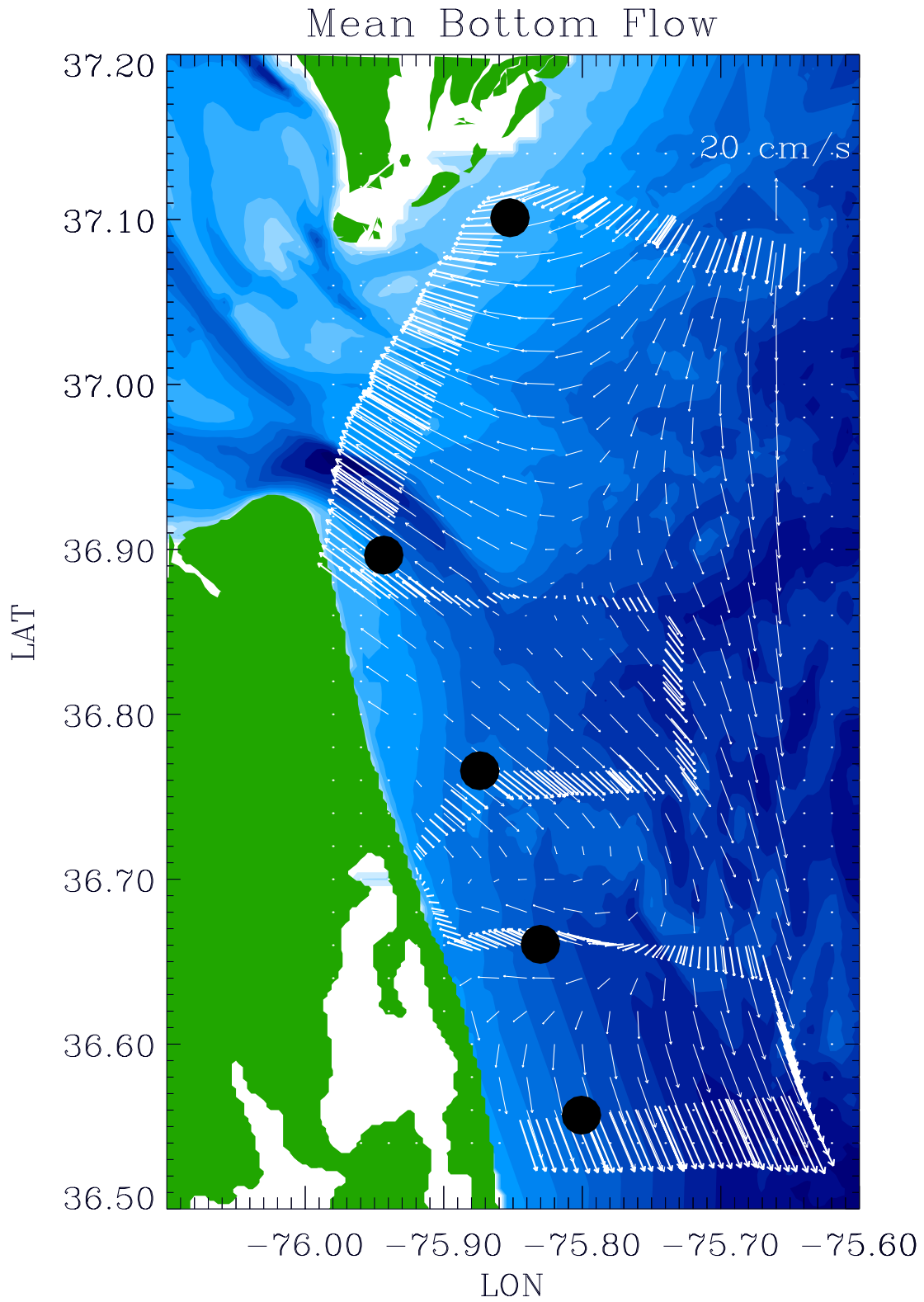


Figure 7(a) Subtidal near-bottom (last usable ADCP bin) flow (vectors) plotted over the bathymetry of the study region. The nodes that anchor the fit are shown as filled circles.

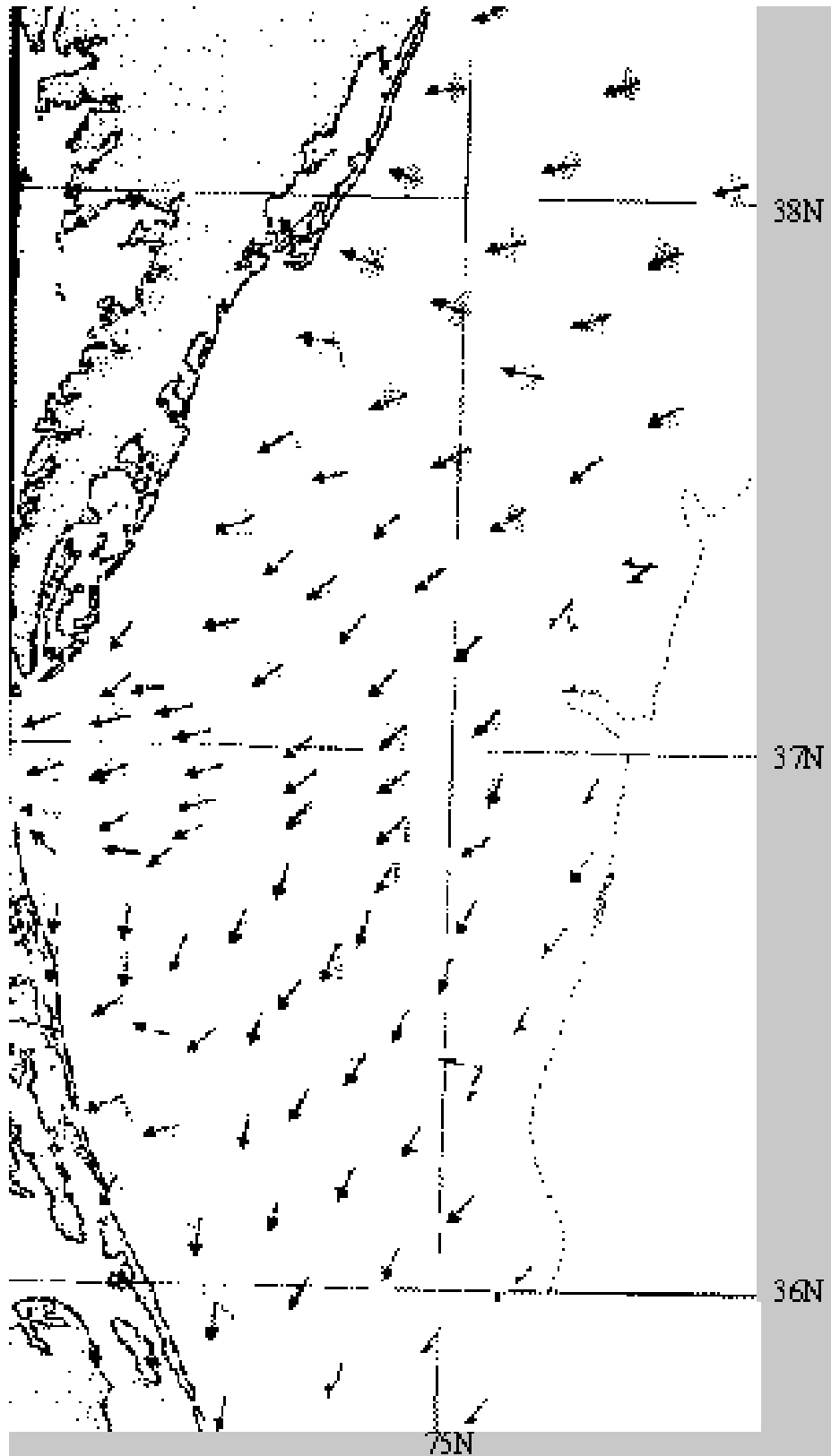


Figure 7(b) Bottom drift derived from seabed drifter recoveries (from Norcross and Stanley, 1969).

from frictional influences (wind stress, vertical mixing, and bottom stress) in the alongflow direction. This is in agreement with the ‘slender’ plume discussed by Garvine (1995). Outside of the region where subtidal surface flow opposes bottom flow, the momentum balance is probably frictional with the wind stress being balanced by the bottom stress. The suggested dynamics within the distinct regions is consistent with the numerical experiments of Valle-Levinson *et al.* (1996).

In addition to the estimate of vertical difference in the subtidal flows, the horizontal divergence of the near-surface flow was calculated to characterize the regions of plume influence. The divergence field (Fig. 8b) showed a zone of positive values (divergent flow) off the mouth of the Chesapeake Bay. Most of this region overlaps with that of large vertical difference in the subtidal flows. Also, the transition from convergence to divergence to the north of the bay mouth is suggestive of the plunging of the ambient flow underneath the plume as proposed above.

#### **4 SUMMARY**

This was the first study that involved underway ADCP measurements of the Chesapeake Bay plume. The ADCP data was separated into subtidal and semidiurnal components with the statistical method previously used by Wong and Münchow (1995) for the Delaware coastal current. Further efforts on separating tidal from subtidal flows should involve dynamically consistent methods such as that outlined by Dowd and Thompson (1996) and compare the results to the statistical method. The present study was carried out under downwelling winds that produced the response diagnosed by modeling results, *i.e.*, buoyant fluid constrained to a narrow band and subtidal flow in the direction of the wind. A main finding of this study is the advection of the turning region of the plume downwind of the estuary mouth by the downwind ambient flow. Also, the observations of this study support the idea of separation of regions with different dynamics based on the surface to bottom difference in subtidal currents. This idea is summarized in Figure 9.

#### **Acknowledgments**

This work was supported by the U.S. Minerals Management Service under Cooperative Agreement No. 14-35-0001-30807. Thanks to the personnel onboard NOAA’s ship Ferrel under the able command of LCDR Susan McKay for their help during the cruise. Tom Wilson and R.C. Kidd were responsible for the technical aspects of the data collection. Andreas Münchow helped us understand the detiding technique. Animations of the near-surface and near-bottom flow, as well as color versions of some of the figures shown here, can be seen at the URL <http://www.ccpo.odu.edu/~arnoldo/tfocbm/tfocbm.html>

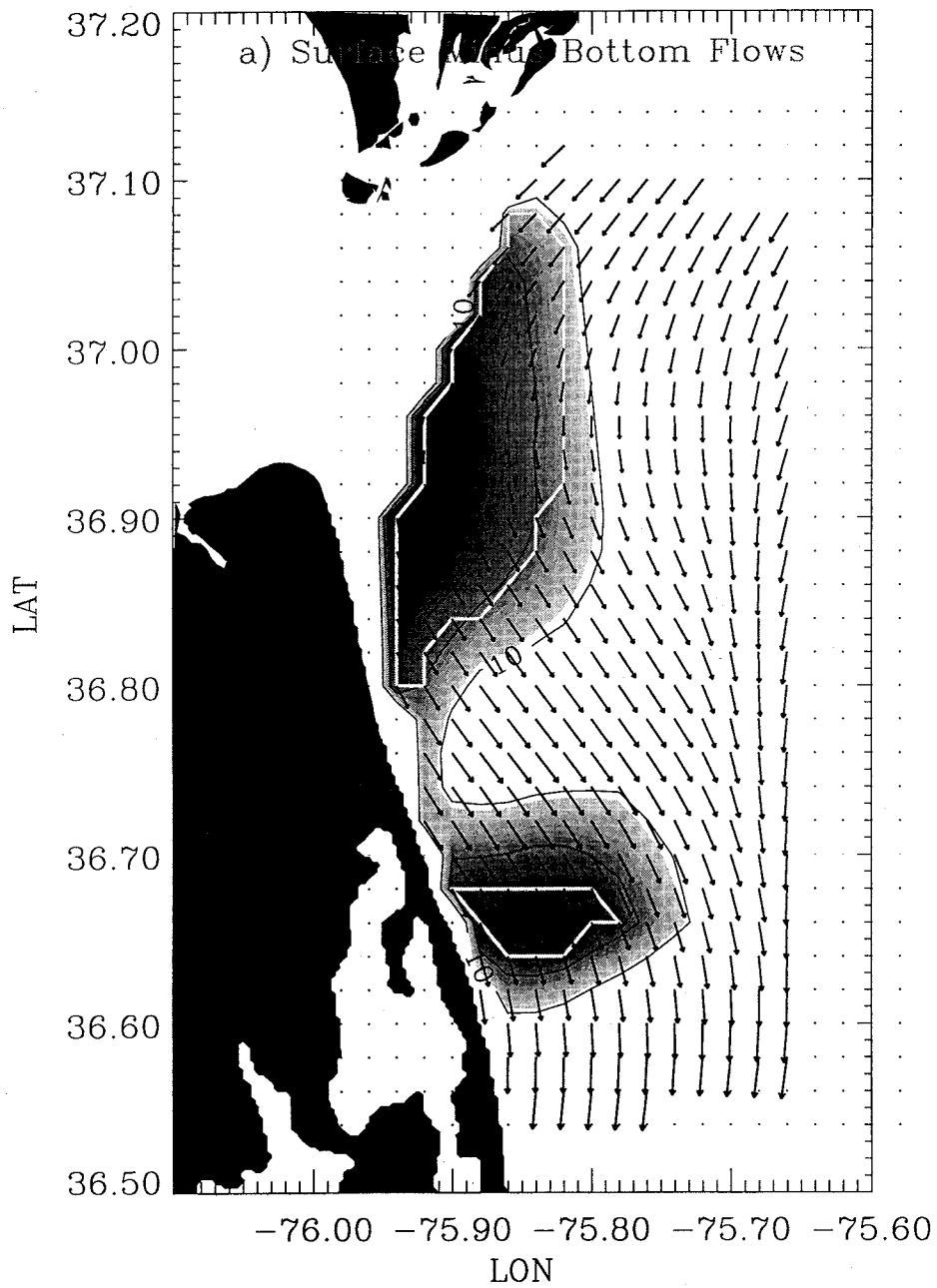


Figure 8(a). Difference between near-surface and near-bottom subtidal flows (dark shades), compared to the near-surface subtidal flow (vectors). The regions with opposing N-S flows at the surface and bottom are within the white-contoured area.

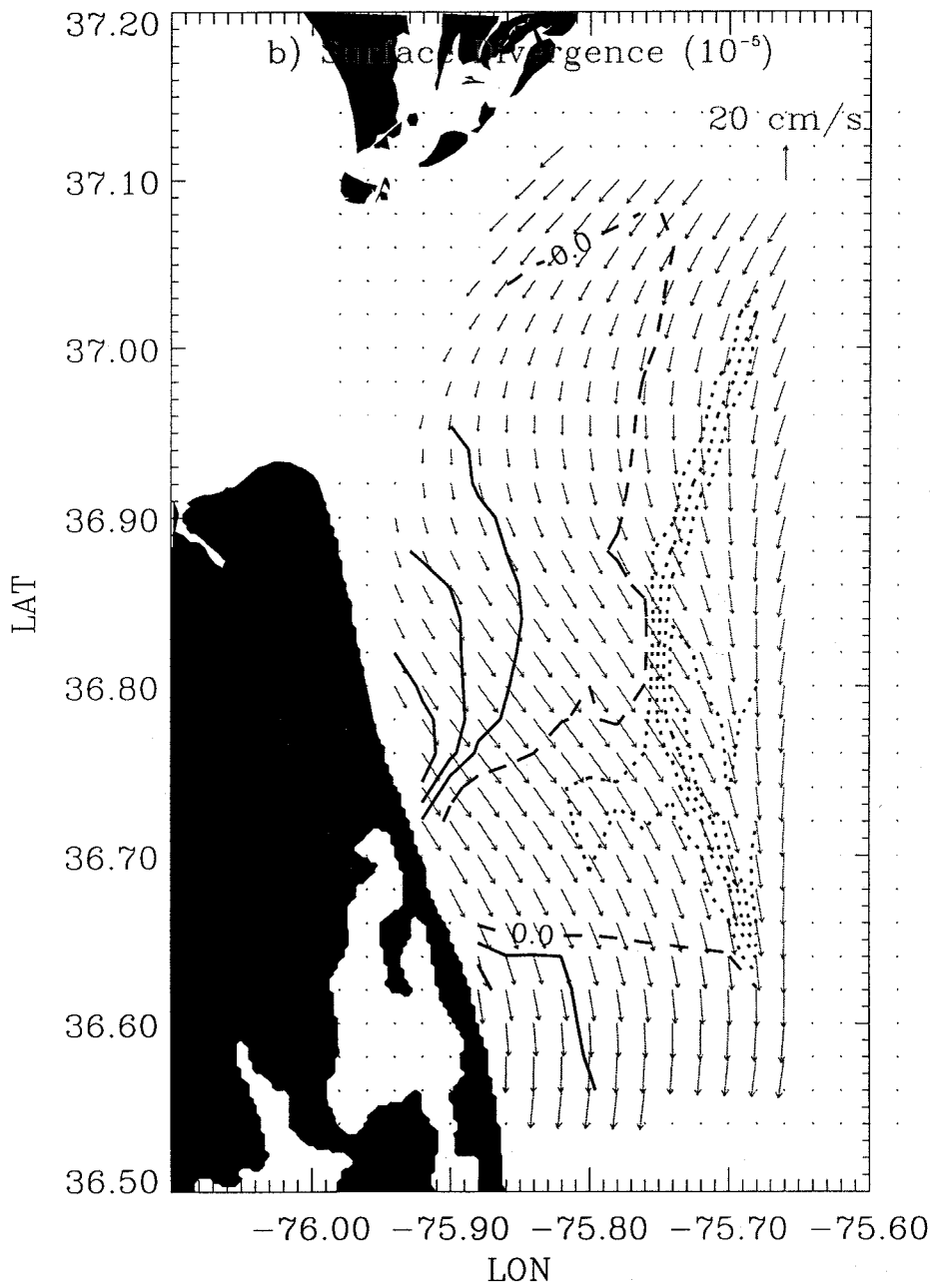


Figure 8 (b). Contours of surface divergence at intervals of  $0.5 \times 10^{-5} \text{ s}^{-1}$ , compared to the near-surface subtidal flow (vectors).

## SUMMARY

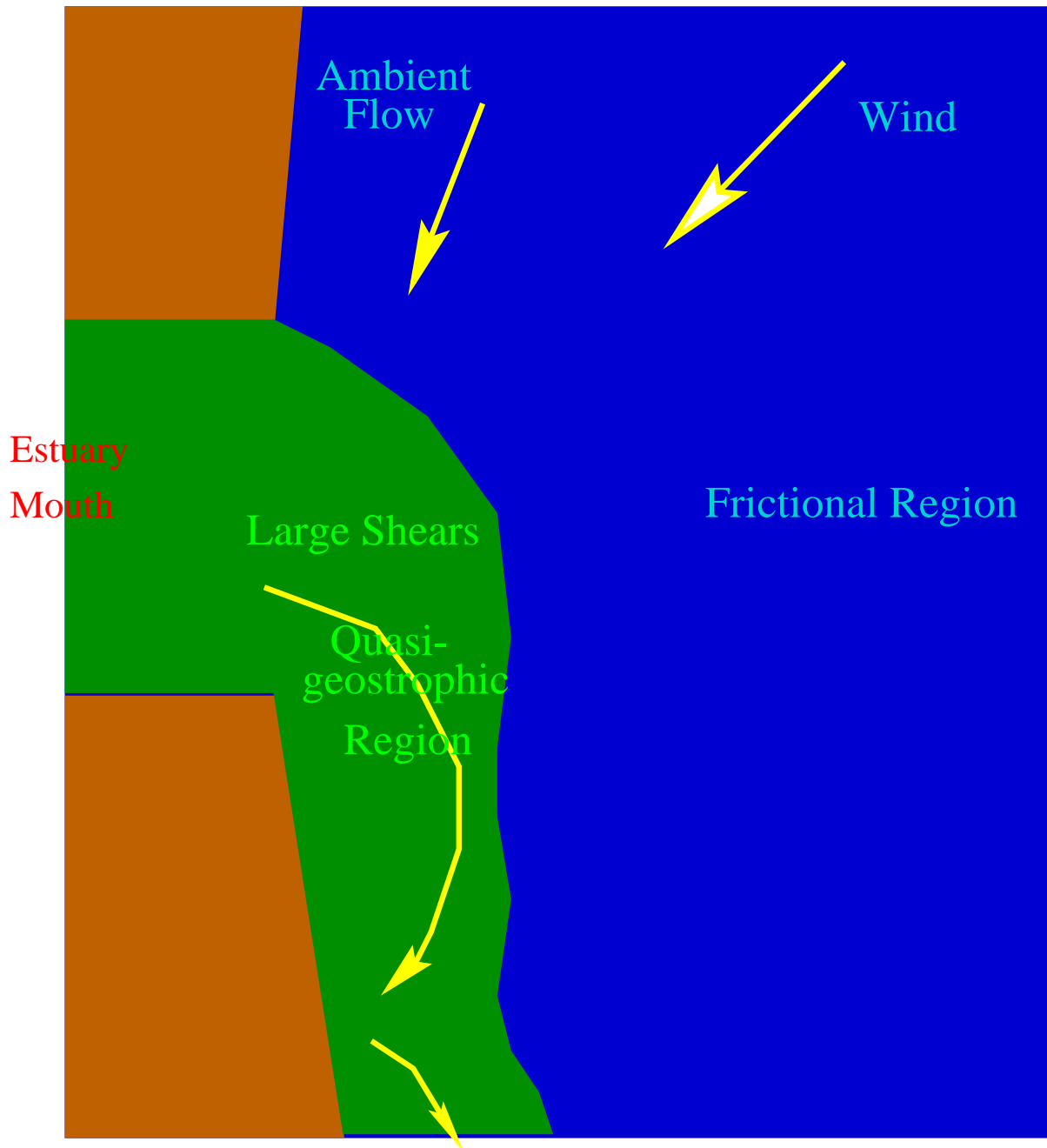


Figure 9. Schematics of the influence on down welling winds on the dynamics of a plume discharging onto the coastal ocean based on the observations.

## REFERENCES

- Boicourt, W.C. 1973. The circulation of water on the continental shelf from Chesapeake Bay to Cape Hatteras. Johns Hopkins Univ. Ph.D. Dissertation. 183 pp.
- Boicourt, W.C. 1981. Circulation in the Chesapeake Bay entrance region: estuary-shelf interaction. In J. Campbell and J. Thomas (eds), Chesapeake Bay Plume Study: Superflux 1980. NASA Conference Publication 2188: 61-78.
- Boicourt, W.C., S.Y. Chao, H.W. Ducklow, P.M. Gilbert, T.C. Malone, M.R. Roman, L.P. Sanford, J.A. Fuhrman, C. Garside, and R.W. Garvine 1987. Physics and microbial ecology of a buoyant estuarine plume on the continental shelf. *Trans. Amer. Geophys. Union*. 68(31): 666-668.
- Candela, J. M., R.C. Beardsley, and R. Limeburner 1992. Separation of tidal and subtidal currents in ship-mounted acoustic Doppler current profiler (ADCP) observations. *J. Geophys. Res.* 97: 769-788.
- Chao, S.-Y. 1988. River-forced estuarine plumes. *J. Phys. Oceanogr.* 18: 72-88.
- Chao, S.-Y. and W.C. Boicourt 1986. Onset of estuarine plumes. *J. Phys. Oceanogr.* 16: 2137-2149.
- Dowd, M. and K.R. Thompson 1996. Extraction of tidal streams from a ship-borne acoustic Doppler current profiler using a statistical-dynamical model. *J. Geophys. Res.* 101(C4): 8943-8956.
- Garvine, R.W. 1995. A dynamical system for classifying buoyant coastal discharges. *Cont. Shelf Res.* 15(13):1585-1596.
- Hargis, W.J. 1981. A benchmark multi-disciplinary study of the interaction between the Chesapeake Bay and adjacent waters of the Virginian sea. In J. Campbell and J. Thomas (eds). Chesapeake Bay Plume Study: Superflux 1980. NASA Conference Publication 2188: 1-14.
- Norcross, J.J. and E.M. Stanley 1969. Inferred surface and bottom drift. In: Circulation of shelf waters off the Chesapeake Bight, W. Harrison, J.J. Norcross, N.A. Pore, and E.M. Stanley (eds). U.S. Dept. of Comm., Environ. Sci. Serv. Admin. Prof. Paper 3: 11-42.
- O'Donnell, J. 1990. The formation and fate of a river plume: A numerical model. *J. Phys. Oceanogr.* 20: 551-569.
- Oey, L.Y., and G.L. Mellor 1993. Subtidal variability of estuarine outflow plume, and coastal current: a model study. *J. Phys. Oceanogr.* 23: 164-171.
- Valle -Levinson, A., 1995 Barotropic and baroclinic exchanges in the lower Chesapeake Bay. *Cont. Shelf Res.* 15: 1631-1647.
- Valle -Levinson, A., J.M. Klinck, and G.H. Wheless 1996. Inflows/outflows at the transition between a coastal plain estuary and the coastal ocean. *Cont. Shelf Res.* 16: 1819-1847.
- Valle-Levinson, A. and K.M.M. Lwiza 1997a. Bathymetric influences on the lower Chesapeake Bay hydrography. *J. Mar. Syst.* 12: 221-236.
- Valle-Levinson, A. and K.M.M. Lwiza 1997b. Rapid assessment of current velocities in the coastal ocean. *Proc. SACLANT Rapid Env. Asst. Conf.* Lerici, Italy.
- Weaver, A.T. and W.W. Hsieh 1987. The influence of buoyancy flux from estuaries on continental shelf circulation. *J. Phys. Oceanogr.* 17: 2127-2140.
- Wiseman, W.J. Jr. and R. W. Garvine 1995. Plumes and coastal currents near large river mouths. *Estuaries.* 18(3): 509-517.

- Wong, K.-C. and A. Mhncow 1995. Buoyancy forced interaction between estuary and inner shelf: observation. *Cont. Shelf Res.* 15(1): 59-88.
- Zhang, Q.H., G.S. Janowitz, and L.J. Pietrafesa 1987. The interaction of estuarine and shelf waters: A model and applications. *J. Phys. Oceanogr.* 17: 455-469.